

Thermodynamic favourability of 1T phase over 1H phase in group III metal monochalcogenide zigzag nanoribbons

Emin Aliyev,¹ Arash Mobaraki,¹ Hâldun Sevinçli,² and Seymur Jahangirov^{1, *}

¹UNAM-Institute of Materials Science and Nanotechnology, Bilkent University, Ankara 06800, Turkey

²Department of Physics, Bilkent University, Ankara 06800, Turkey

(Dated: January 14, 2025)

Owing to the promising optoelectric and thermoelectric properties of two-dimensional (2D) group III-VI materials (MXs), their nanoribbons (NRs) have attracted notable attention as an emerging class of quasi-one-dimensional (quasi-1D) nanostructures. Due to the fact that the most stable 2D monolayer polymorph of MXs is the 1H phase, to date, existing studies in the literature have predominantly focused on the NRs formed from 1H phase MXs. Nevertheless, NRs of the 1T phase have received little to no attention. Employing ab initio simulations based on density functional theory, we systematically compared the thermodynamic stability of hydrogen passivated and unpassivated 1T and 1H ZNRs of GaS, GaSe, and InSe. Our results reveal that 1T phase MX ZNRs are thermodynamically favorable at widths up to 34 nm, a range that is realizable through contemporary experimental fabrication techniques. Furthermore, unlike metallic 1H ZNRs, 1T ZNRs remain semiconductor and retain a Mexican-hat-shaped top valence band without any built-in potential between the edges. Complementarily, hydrogenation energies of 1T InSe ZNRs are positive, and due to the edge-localized states, the 1T unpassivated ZNRs possess nearly flat top valence bands. Our findings serve as a compass for subsequent synthesis pathways of group III-VI NRs.

Keywords: Nanoribbons, Phase transition, Metal monochalcogenides, Electronic band structure

I. INTRODUCTION

Since the isolation of 2D graphene monolayer from graphite [1], exploration of low-dimensional structures have attracted considerable attention of researchers. Among these structures, 2D group III metal monochalcogenides (MXs, $M = \text{Ga, In}$, and $X = \text{S, Se}$) are attracting heightened interest due to the remarkable variety of polymorphs with distinct physical properties [2–9]. Unlike common 2D materials, they exhibit extraordinary non-parabolic inverted Mexican-hat-shaped band structure at the valence band maximum, which leads to flatter energy distribution, resulting in a van Hove singularity in the density of states [10, 11]. The ground state of these MXs is hexagonal (H) phase (D_{3h} point group), where a unit cell consists of metal atoms sandwiched between chalcogen atoms in X-M-M-X atomic arrangement. Few-layer and monolayer 2D structures of H-phase GaS, GaSe, and InSe were successfully synthesized with various methods [12–15]. A recent study [16] reported fabrication of ballistic field effect transistor (FET) with mechanically exfoliated 2D InSe, that outperformed any previously reported silicon FETs. In addition to FETs, studies report great potential of H-phase MXs in the fields of optoelectronics, spintronics, and thermoelectrics [13, 17].

Moreover, numerous theoretical investigations [9, 18, 19] have shown that MXs can also crystallize in metastable staggered T phase (D_{3d} point group), which is energetically quasi-degenerate phase, as the energy difference between H and T phases is less than $k_B T$ at room temperature and can be traversed with strain or doping.

The T phase structurally is similar to the H phase, with an exception of the atomic environment of the chalcogen atoms: in the X-M-M-X tetralayer the upper X atoms layer is rotated by 60° with respect to the lower one (see Fig. 1) [19]. In a recent study [3], T-phase 2D GaS films were fabricated by chemical vapor deposition method. Furthermore, T-phase GaSe 2D layers were fabricated using molecular beam epitaxy method [2, 8]. In addition, 2D GaSe with T-phase-like layers formed due to intralayer sliding of Se atoms was reported to exhibit exotic nonvolatile memory behavior with a high channel current on/off ratio [4].

While 2D materials exhibit great potential and unique properties, by confining these 2D layers laterally [20, 21], one can obtain quasi-1D nanoribbons (NRs), which lead to the emergence of a broader spectrum of properties and enable fine-tuning of these properties by altering the width [22], edge shapes, and various edge functionalizations of ribbons [23, 24]. Such adaptability and size made NRs attractive candidates for nanoscale applications in various fields, including spintronics [25], optoelectronics [26, 27], catalysis [28], and biomedical applications [29]. Due to their intriguing properties and diverse applications, investigating the possible phase transition has been previously explored in NRs to expand the scope of their potential applications [30]. Such phase transitions are typically influenced by applying external electric and magnetic fields or imposing mechanical forces [31–36]. Furthermore, it has been demonstrated that the phase stability and electronic properties can be affected by the width of NRs [37–41].

The distinguishing properties of 2D MXs inspired many researchers to investigate their 1D counterparts as well. To date, various 1D MX nanostructures, such as

* seymur@unam.bilkent.edu.tr

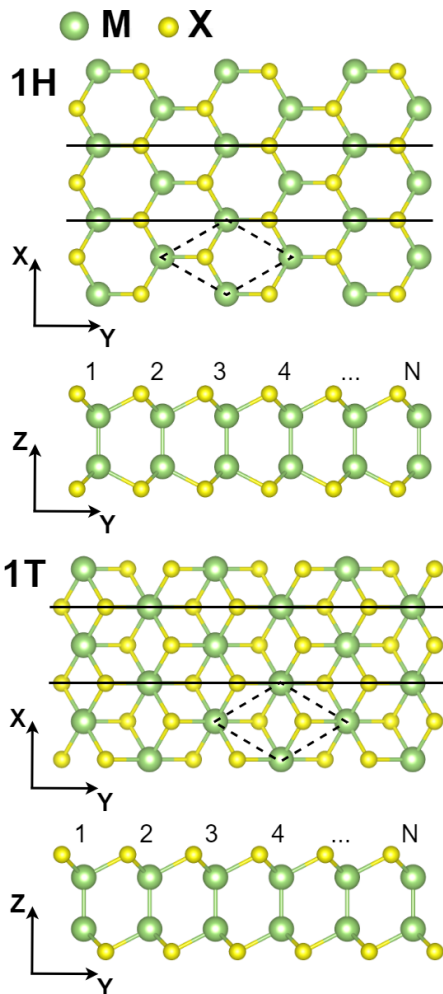


FIG. 1. Schematic representations of 1T and 1H MX NRs and the unit cells of the corresponding 2D monolayers.

nanobelts, nanowires, and NRs, have been fabricated and demonstrated to exhibit promising properties for the next generation of nanophotonics and optoelectronics [42–49]. Besides, 1H MX NRs were subjected to several theoretical studies that reported peculiar electronic and magnetic properties, such as intrinsic ferromagnetism (FM) in GaS NRs with zigzag edge (ZNRs) [50, 51]. Notably, FM state in GaS ZNRs prevails even under tensile and compressive strains, with transition to AFM state being observed only at high compressive strains [52]. H-passivation also significantly affects the electronic properties of GaS NRs. Passivation of the GaS armchair-edge NRs results in an increase of band gap by 1 eV to 2.48 eV, which remains practically constant with increasing width [53]. On the other hand, GaS ZNRs are reported to remain metallic even after passivation with H, except at very narrow widths ($N \leq 4$) [53]. A different study reported comparable trends in the electronic properties of GaSe NRs, closely aligning with the observations in GaS NRs [54]. In addition, InSe ZNRs are also reported to be metallic

and exhibit promising catalytic performance in hydrogen evolution reaction [55, 56].

While all of the studies mentioned above have focused on the 1H MX NRs, the 1T MX NRs remain overlooked in the existing literature. In this paper, utilizing ab initio simulations based on density functional theory (DFT) [57, 58], we carried out a systematic analysis to explore the width-dependent variations in the energy difference between the 1T and 1H phases of MX ZNRs. Our investigation uncovers that in both cases of hydrogen-passivated ZNRs (P-ZNRs) and unpassivated ZNRs (UP-ZNRs), the 1T ZNRs are thermodynamically more favorable up to critical widths of about 23, 31, and 34 nm in the cases of GaS, GaSe, and InSe, respectively. Notably, 1T ZNRs are semiconductors with no built-in potential between their edges.

II. COMPUTATIONAL DETAILS

All DFT calculations in this study were conducted using the Vienna Ab initio Software Package (VASP) [59]. We employed projector augmented-wave pseudopotentials [60, 61] within the generalized gradient approximation of Perdew, Burke, and Ernzerhof [62–64], with spin polarization considered. Ribbons are placed in the x-y plane (see Fig. 1), and a vacuum of 15 Å is considered in non-periodic directions to eliminate interactions with images. The structures are fully relaxed using kinetic energy cutoff of 500 eV for the plane-wave basis and a Γ -centered $10 \times 1 \times 1$ k-point mesh is used for sampling the Brillouin zone (BZ). The convergence tolerance for the total energy of the system is set to be less than 10^{-7} eV, and the Hellmann-Feynman forces are minimized to be less than 10^{-2} eV/Å.

III. RESULTS AND DISCUSSIONS

Defining N as the number of the 2D monolayer unit cells forming the NR, we studied MX ZNRs ranging from $N = 4$ to $N = 14$. As summarized in Table. S1, the calculated structural parameters and energy differences between the considered 2D MXs show perfect agreement with previous reports [19, 65]. Besides, with increasing N , the lattice constants of the relaxed ZNRs converge toward the 2D monolayer lattice constants (see Fig. S1).

Fig. 2 illustrates the variation of the total ground state energy differences between the MX ZNRs of the 1H and 1T phases ($\Delta E = E_{1H} - E_{1T}$) as a function of N . The first noteworthy result deduced from this graph is that contrary to corresponding 2D monolayers, ΔE is positive in ZNRs of considered widths, which indicates the thermodynamic favorability of the 1T phase. However, with increasing width, we observe a linear decrease in the ΔE of UP-ZNRs, while in the case of P-ZNRs, the ΔE starts to decrease after reaching a maximum value. Such behavior is expected, since at a certain critical width,

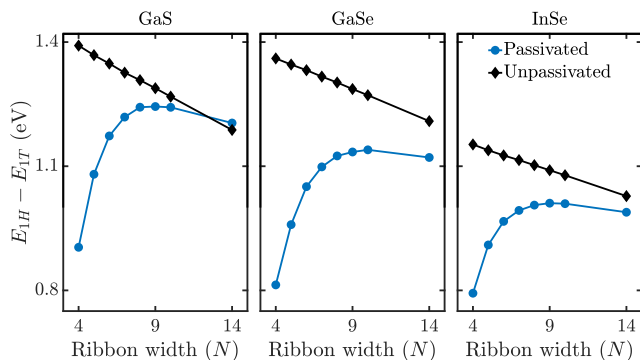


FIG. 2. Energy difference between the 1H and 1T phases in passivated (blue circles) and unpassivated (black diamonds) cases with respect to N . Lines are guides for the eye.

the 1H should take over the 1T phase ($\Delta E < 0$). As described in ref [38], this critical width can be determined by utilizing the formation energy of NRs. The formation energy for UP-NRs can be expressed as:

$$E_{form}(N) = E_r(N) - NE_{2D} \quad (1)$$

where $E_r(N)$ is the total energy of the NR, E_{2D} is the energy per formula unit of the corresponding 2D monolayer. For P-NRs, the formation energy of two hydrogen molecules is subtracted from the right side of Eq. 1. Subsequently, the converged values of E_{form}^{1H} and E_{form}^{1T} can be used to determine N_c as follows:

$$N_c = \frac{E_{form}^{1H} - E_{form}^{1T}}{E_{2D}^{1T} - E_{2D}^{1H}} \quad (2)$$

The formation energies as a function of N are presented in Fig. S2, and the calculated N_c values are given in Table I. The minimum N_c is 72 (23 nm), which is found in the case of GaS P-ZNRs, and the maximum obtained value is 95 (34 nm), corresponding to InSe UP-ZNRs, significantly larger width compared to TMD NRs, where the maximum reported N_c is 7 [38, 39]. Notably, the predicted widths are achievable by state of the art fabrication methods [43, 44, 48, 66].

TABLE I. The calculated values of critical width in terms of N_c (defined in Eq. 2) where the crossover between the 1T and 1H phases of MX ZNRs occurs. The approximate width (W in nm) is calculated using the lattice constant of the corresponding 1H 2D monolayer.

	Unpassivated		Passivated	
	N_c	W (nm)	N_c	W (nm)
GaS	73	23	72	23
GaSe	93	31	87	29
InSe	95	34	92	33

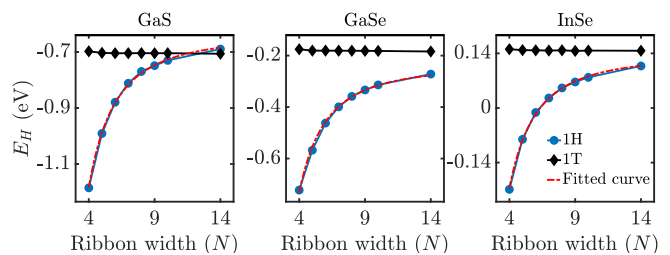


FIG. 3. The calculated hydrogenation energies of 1T (black diamonds) and 1H (blue circles) MX ZNRs as a function of width. Solid lines are guides for the eye. The red dashed lines are $\frac{\alpha}{N^2} + \beta$ fits for describing the nonlinear behavior of 1H ZNRs.

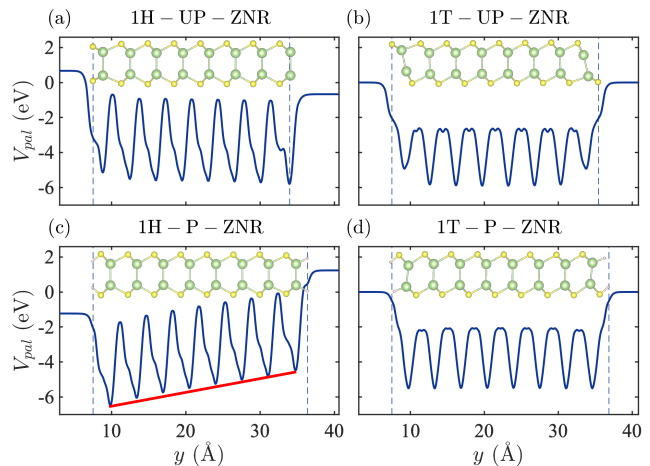


FIG. 4. Planar average of the local electrostatic potential of (a) unpassivated 1H, (b) unpassivated 1T, (c) passivated 1H, and (d) passivated 1T $N = 8$ InSe ZNRs. Vertical dashed lines show the position of the first and last atom along the width of the NRs.

The hydrogenation energies (E_H) depicted in Fig. 3 give further insight into the nonlinear behavior of ΔE of passivated ZNRs. While the E_H of 1T ZNRs remains practically constant, in the case of 1H ZNRs, the ΔE exhibits a nonlinear behavior that can be approximated by $\frac{\alpha}{N^2} + \beta$, as shown by the dashed red lines in Fig. 3. The origin of this nonlinearity in E_H can be deduced from Fig. S2, where the E_{form} of 1H-P-ZNRs exhibits a nonlinear behavior, while in the case of 1H-UP-ZNRs, it is practically constant. Another distinct feature of 1H-P-ZNRs can be seen in planar averaged local potentials (V_{pal}) presented in Figs. 4, S4, and S5. Along the width of ZNRs, we observe oscillation in V_{pal} with almost the same extrema except for the 1H-P-ZNRs, where there is practically a linear change of extrema, a behavior that was previously observed in the case of polar surfaces [67, 68] and NRs [69]. An additional noteworthy feature that can be deduced from Fig. 4 is the presence of a built-in electric field only in 1H ZNRs, which is a key factor in determining thermodynamic stability. As

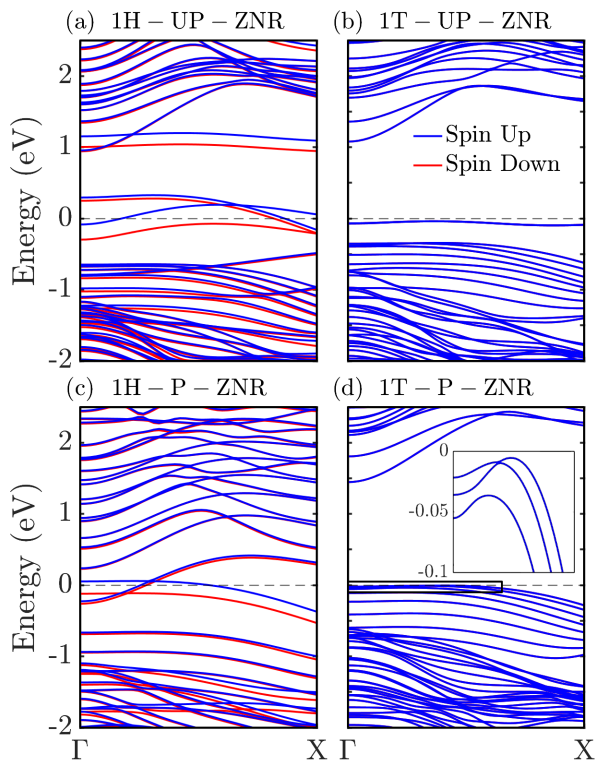


FIG. 5. Spin-polarized band structures of (a) unpassivated 1H, (b) unpassivated 1T, (c) passivated 1H and (d) passivated 1T $N = 8$ InSe ZNRs.

demonstrated by Zhong et al. [70], the stability of ultrathin films is determined by competition between built-in electric field and reconstruction processes, and as the number of layers decreases, the nonpolar thin films become more favorable and compensate for the residual electrostatic energy. In a related context, we observe that the nonpolar MX ZNRs become more stable when the ribbon widths are sufficiently small.

Building on the aforementioned results, we now investigate their implications in relation to the electronic properties of ZNRs. As numerous studies have previously reported [50–55], 1H ZNRs show metallic behavior. On the other hand, our results, as presented in Figs. 5, S6, and S7, reveal that all considered 1T ZNRs retain a band gap regardless of passivation and size. The band gaps of 1T-P-ZNRs show a decreasing trend that converges to 2D monolayer band gaps as the width increases, while the band gaps of UP-ZNRs exhibits no substantial width dependence (see Fig. S3). On top of it, similar to the

2D counterparts, 1T ZNRs possess a Mexican-hat-shaped top valence band. Furthermore, as shown in Figs. 5 (d), S6 (d) and S7 (d), 1T-UP-ZNRs exhibit a nearly flat, edge-localized top valence band (see Fig. S8). Notably, there is an increasing trend in (E_H) as the atomic number of the constituents in MX increases, reaching positive values in the case of InSe ZNRs (Fig. 3), indicating the possibility of 1T InSe ZNRs formation without hydrogen passivation.

CONCLUSION

Employing DFT-based calculations, we thoroughly examined the width-dependent structural and electronic properties of hydrogen passivated and bare MX ZNRs. The remarkable finding of this study is the demonstration of the existing crossover between the 1T and 1H phases. Contrary to 2D monolayers, where 1H is the most thermodynamically favorable phase, in MX ZNRs, the 1T phase is more favorable than 1H, below experimentally achievable critical widths ranging from 23 nm in GaS up to 34 nm in InSe ZNRs. The 1T-UP-ZNRs possess a nearly flat top valence band due to localized edge states, and band gaps that do not show substantial width-dependent variation. In 1T-P-ZNRs, the top valence band retains a Mexican-hat shape akin to their 2D monolayer counterparts, and band gaps exhibit a downward trend toward 2D monolayer values, creating a tunable platform for thermoelectric and optoelectronic applications. Another noteworthy observation is that, unlike 1H ZNRs, there is no built-in potential between the edges in 1T ZNRs. Lastly, positive hydrogenation energies along with nearly flat top valence bands make InSe 1T-UP-ZNRs potential candidates for spintronic and thermoelectric applications. Our results lay the foundation for future experimental investigations.

ACKNOWLEDGMENTS

E.A., A.M. and S.J. acknowledge support from the TÜBİTAK-ANAS project number 120N296. H.S. acknowledges support from the Air Force Office of Scientific Research (AFOSR, Award No. FA9550-21-1-0261). The calculations were performed at TÜBİTAK ULAKBİM, High Performance and Grid Computing Center (TRUBA resources) and National Center for High-Performance Computing of Turkey (UHeM) under grant number 1007742020.

-
- [1] A. K. Geim and K. S. Novoselov, *Nature materials* **6**, 183 (2007).
 [2] M. Yu, S. A. Iddawela, J. Wang, M. Hilse, J. L. Thompson, D. Reifsnyder Hickey, S. B. Sinnott, and S. Law,

ACS nano (2024).

- [3] Y. Gutiérrez, F. Agresti, D. Juan, S. Dicorato, M. M. Giangregorio, F. Moreno, P. García-Fernández, J. Junquera, L. Armelao, and M. Losurdo, *Advanced Optical*

- Materials, 2303002 (2024).
- [4] W. Li, X. Zhang, J. Yang, S. Zhou, C. Song, P. Cheng, Y.-Q. Zhang, B. Feng, Z. Wang, Y. Lu, *et al.*, Nature Communications **14**, 2757 (2023).
 - [5] T. Hu, C. Xu, A. Zhang, and P. Yu, Materials Advances **3**, 2213 (2022).
 - [6] C. Wen, Z. Zhang, Z. Guo, J. Shen, B. Sa, P. Lin, J. Zhou, and Z. Sun, Journal of Physics: Condensed Matter **32**, 065501 (2019).
 - [7] H. Bergeron, D. Lebedev, and M. C. Hersam, Chemical Reviews **121**, 2713 (2021).
 - [8] J. Grzonka, M. S. Claro, A. Molina-Sánchez, S. Sadewasser, and P. J. Ferreira, Advanced Functional Materials **31**, 2104965 (2021).
 - [9] X. Li, L. Li, and M. Wu, Materials Today Physics **15**, 100229 (2020).
 - [10] H. Cai, Y. Gu, Y.-C. Lin, Y. Yu, D. B. Geohegan, and K. Xiao, Applied Physics Reviews **6** (2019).
 - [11] M. N. Çınar, G. Ö. Sargın, K. Sevim, B. Özdamar, G. Kurt, and H. Sevinçli, Physical Review B **103**, 165422 (2021).
 - [12] Z. Yang and J. Hao, Advanced Materials Technologies **4**, 1900108 (2019).
 - [13] M. Yu, M. Hilse, Q. Zhang, Y. Liu, Z. Wang, and S. Law, ACS Applied Nano Materials (2024).
 - [14] D. A. Bandurin, A. V. Tyurnina, G. L. Yu, A. Mishchenko, V. Zólyomi, S. V. Morozov, R. K. Kumar, R. V. Gorbachev, Z. R. Kudrynskyi, S. Pezzini, *et al.*, Nature nanotechnology **12**, 223 (2017).
 - [15] M. Brotons-Gisbert, D. Andres-Penares, J. Suh, F. Hidalgo, R. Abargues, P. J. Rodriguez-Canto, A. Segura, A. Cros, G. Tobias, E. Canadell, *et al.*, Nano letters **16**, 3221 (2016).
 - [16] J. Jiang, L. Xu, C. Qiu, and L.-M. Peng, Nature **616**, 470 (2023).
 - [17] Y. Xiong, D. Xu, Y. Feng, G. Zhang, P. Lin, and X. Chen, Advanced Materials **35**, 2206939 (2023).
 - [18] H. Nitta, T. Yonezawa, A. Fleurence, Y. Yamada-Takamura, and T. Ozaki, Physical Review B **102**, 235407 (2020).
 - [19] J. Zhou and H. L. Zhuang, ChemistrySelect **1**, 5779 (2016).
 - [20] J. Cai, P. Ruffieux, R. Jaafar, M. Bieri, T. Braun, S. Blankenburg, M. Muoth, A. P. Seitsonen, M. Saleh, X. Feng, *et al.*, Nature **466**, 470 (2010).
 - [21] Y. Chen, P. Cui, X. Ren, C. Zhang, C. Jin, Z. Zhang, and C.-K. Shih, Nature communications **8**, 15135 (2017).
 - [22] Y.-W. Son, M. L. Cohen, and S. G. Louie, Physical review letters **97**, 216803 (2006).
 - [23] A. Bellunato, H. Arjmandi Tash, Y. Cesa, and G. F. Schneider, ChemPhysChem **17**, 785 (2016).
 - [24] L. Talirz, H. Söde, J. Cai, P. Ruffieux, S. Blankenburg, R. Jafaar, R. Berger, X. Feng, K. Müllen, D. Passerone, *et al.*, Journal of the American Chemical Society **135**, 2060 (2013).
 - [25] Z. Wang, D. Fan, M. Yin, H. Li, H. Hu, F. Guo, Z. Feng, J. Li, D. Zhang, Z. Li, *et al.*, New Journal of Chemistry **48**, 4699 (2024).
 - [26] S. Kumar, S. Pratap, V. Kumar, R. K. Mishra, J. S. Gwag, and B. Chakraborty, Luminescence **38**, 909 (2023).
 - [27] Z. He, K. Wang, C. Yan, L. Wan, Q. Zhou, T. Zhang, X. Ye, Y. Zhang, F. Shi, S. Jiang, *et al.*, ACS Applied Materials & Interfaces **15**, 7148 (2023).
 - [28] M. Aparna and R. Chatanathodi, Applied Surface Science **618**, 156677 (2023).
 - [29] H. Hou, L. Cardo, J. Merino, F. Xu, C. Wetzl, B. Arnaiz, X. Luan, Y. Mai, A. Criado, and M. Prato, Materials Today Chemistry **33**, 101668 (2023).
 - [30] J. Li, S. Sanz, N. Merino-Díez, M. Vilas-Varela, A. Garcia-Lekue, M. Corso, D. G. de Oteyza, T. Frederiksen, D. Peña, and J. I. Pascual, Nature communications **12**, 5538 (2021).
 - [31] A. Huang, S. Ke, J.-H. Guan, J. Li, and W.-K. Lou, Physical Review B **109**, 045408 (2024).
 - [32] X. L. Lü, Y. Xie, and H. Xie, New Journal of Physics **20**, 043054 (2018).
 - [33] S. Sivasubramani, S. Debroy, S. G. Acharyya, and A. Acharyya, Nanotechnology **29**, 455701 (2018).
 - [34] Y. Xie, B. Wang, L. Zhang, X. Wang, H. Yang, G. Li, and R.-W. Li, Journal of Magnetism and Magnetic Materials **573**, 170674 (2023).
 - [35] Y. Yang, H. Zong, X. Ding, and J. Sun, Applied Physics Letters **121** (2022).
 - [36] D. Popple, M. Dogan, T. V. Hoang, S. Stonemeyer, P. Ercius, K. C. Bustillo, M. Cohen, and A. Zettl, Physical Review Materials **7**, L013001 (2023).
 - [37] Y. Hong, J. Deng, X. Ding, J. Sun, and J. Z. Liu, The Journal of Physical Chemistry Letters **14**, 3160 (2023).
 - [38] F. Güller, A. M. Llois, J. Goniakowski, and C. Noguera, Physical Review B **91**, 075407 (2015).
 - [39] W. Zan, Z. Zhang, Y. Yang, X. Yao, S. Li, and B. I. Yakobson, Nanotechnology **30**, 075701 (2018).
 - [40] W.-Y. Zan, J. Huo, Y.-W. Mu, and S.-D. Li, Applied Surface Science **599**, 153949 (2022).
 - [41] A. D. Zdetsis, Carbon **210**, 118042 (2023).
 - [42] P. Sutter, J. S. French, L. Khosravi Khorashad, C. Argypoulos, and E. Sutter, Nano letters **21**, 4335 (2021).
 - [43] P. Hauchecorne, F. Gity, M. Martin, H. Okuno, S. Bhattacharjee, J. Moeyaert, D. Rouchon, B. Hyot, P. K. Hurley, and T. Baron, ACS Applied Nano Materials **4**, 7820 (2021).
 - [44] E. Sutter, J. S. French, S. Sutter, J. C. Idrobo, and P. Sutter, ACS nano **14**, 6117 (2020).
 - [45] C.-Y. Wu, H. Zhu, M. Wang, J. Kang, C. Xie, L. Wang, and L.-B. Luo, Journal of Materials Chemistry C **8**, 5375 (2020).
 - [46] X. Xiong, Q. Zhang, X. Zhou, B. Jin, H. Li, and T. Zhai, Journal of Materials Chemistry C **4**, 7817 (2016).
 - [47] G. Shen, D. Chen, P.-C. Chen, and C. Zhou, Acs Nano **3**, 1115 (2009).
 - [48] S. K. Panda, A. Datta, G. Sinha, S. Chaudhuri, P. G. Chavan, S. S. Patil, M. A. More, and D. S. Joag, The Journal of Physical Chemistry C **112**, 6240 (2008).
 - [49] H. Arora and A. Erbe, InfoMat **3**, 662 (2021).
 - [50] B.-J. Wang, X.-H. Li, L.-W. Zhang, G.-D. Wang, and S.-H. Ke, Chinese Physics B **25**, 107101 (2016).
 - [51] Y. Zhou, S. Li, W. Zhou, X. Zu, and F. Gao, Scientific reports **4**, 5773 (2014).
 - [52] B.-J. Wang, X.-H. Li, L.-W. Zhang, G.-D. Wang, and S.-H. Ke, Chinese Physics B **26**, 057102 (2017).
 - [53] M. Mosafery, I. A. Sarsari, and M. Alaei, Applied Physics A **127**, 123 (2021).
 - [54] J. Zhou, RSC advances **5**, 94679 (2015).
 - [55] M. Wu, J.-j. Shi, M. Zhang, Y.-m. Ding, H. Wang, Y.-l. Cen, W.-h. Guo, S.-h. Pan, and Y.-h. Zhu, Nanotechnology **29**, 205708 (2018).

- [56] X. Cheng, C. Zhang, L. Guan, and J. Tao, *International Journal of Hydrogen Energy* **44**, 24174 (2019).
- [57] P. Hohenberg and W. Kohn, *Physical review* **136**, B864 (1964).
- [58] W. Kohn and L. J. Sham, *Physical review* **140**, A1133 (1965).
- [59] G. Kresse and J. Furthmüller, *Physical review B* **54**, 11169 (1996).
- [60] G. Kresse and D. Joubert, *Physical review b* **59**, 1758 (1999).
- [61] P. E. Blöchl, *Physical review B* **50**, 17953 (1994).
- [62] J. P. Perdew, K. Burke, and M. Ernzerhof, *Physical review letters* **77**, 3865 (1996).
- [63] G. Kresse and J. Hafner, *Physical review B* **47**, 558 (1993).
- [64] G. Kresse and J. Furthmüller, *Computational materials science* **6**, 15 (1996).
- [65] V. Zólyomi, N. Drummond, and V. Fal'Ko, *Physical Review B* **89**, 205416 (2014).
- [66] M. A. Aslam, T. H. Tran, A. Supina, O. Siri, V. Meunier, K. Watanabe, T. Taniguchi, M. Kralj, C. Teichert, E. Sheremet, *et al.*, *npj 2D Materials and Applications* **6**, 76 (2022).
- [67] J.-H. Song, T. Akiyama, and A. J. Freeman, *Physical Review B—Condensed Matter and Materials Physics* **77**, 035332 (2008).
- [68] J. Li, J. Gayles, N. Kioussis, Z. Zhang, C. Grein, and F. Aqariden, *Journal of electronic materials* **41**, 2745 (2012).
- [69] A. Yamanaka and S. Okada, *Physical Chemistry Chemical Physics* **19**, 9113 (2017).
- [70] Z. Zhong, G. Koster, and P. J. Kelly, *Physical Review B—Condensed Matter and Materials Physics* **85**, 121411 (2012).

SUPPLEMENTARY MATERIAL

TABLE S1. The calculated energy differences (ΔE) between 1T and 1H phase of 2D MXs and lattice constants of the structures are compared with previous works.

Material	This Work			Previous Work			Ref
	ΔE (meV)	1H Lattice Constant (\AA)	1T Lattice Constant (\AA)	ΔE (meV)	1H Lattice Constant (\AA)	1T Lattice Constant (\AA)	
GaS	20	3.63	3.64	20	3.63	3.64	[19]
GaSe	15	3.82	3.83	15	3.82	3.83	[19]
InSe	13	4.09	4.09	13	4.09	4.09	[65]

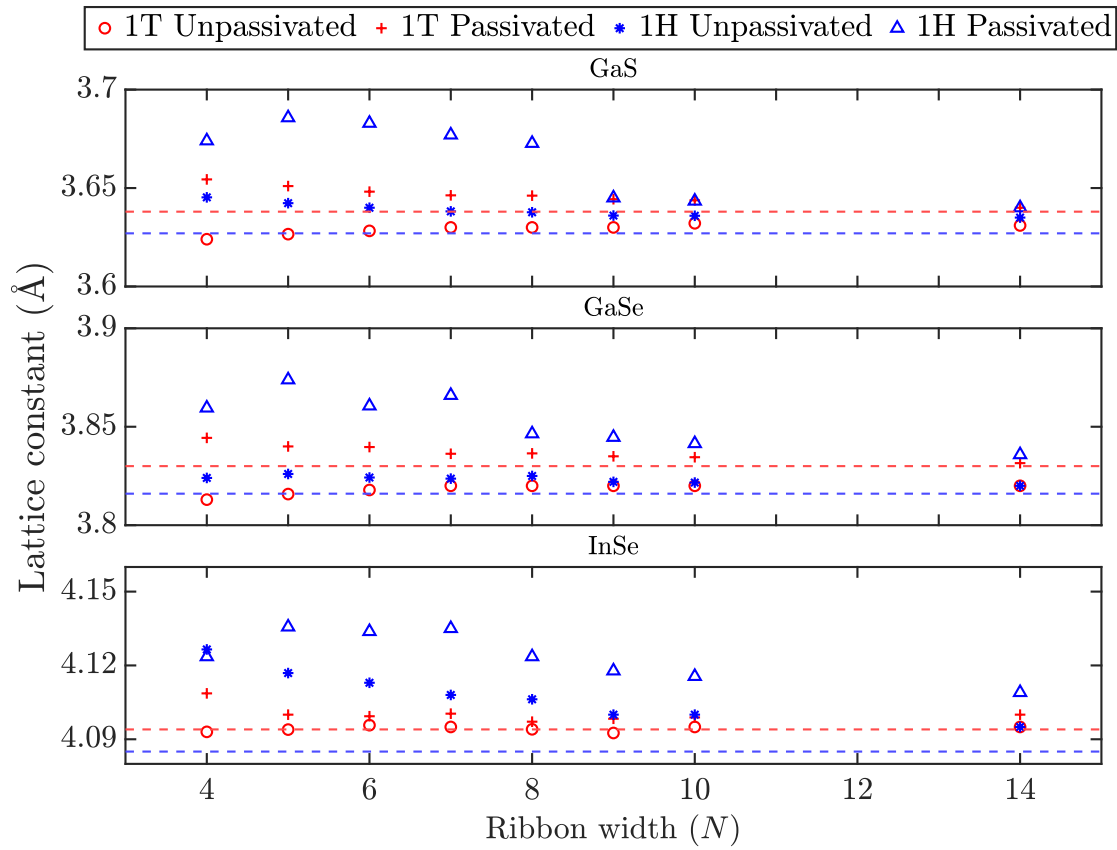


FIG. S1. Variation of the calculated lattice constants of MX ribbons with ribbon width. Red and blue dashed lines show the calculated lattice constants of 2D 1T and 1H MXs, respectively.

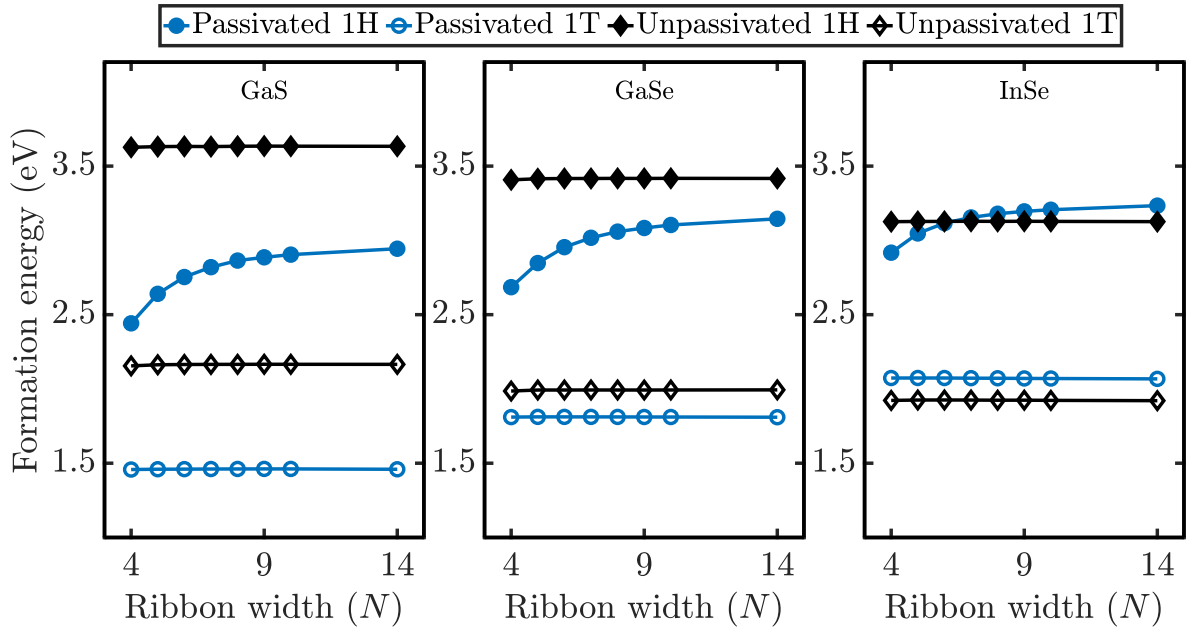


FIG. S2. Calculated formation energies of MX NRs plotted against ribbon width. Solid Lines are guides for the eye.

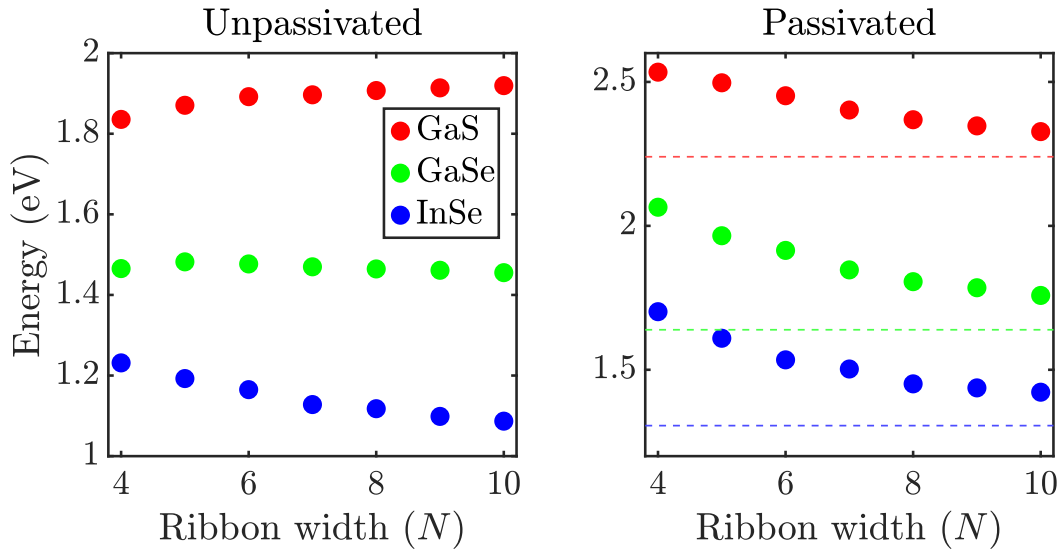


FIG. S3. Variation of the bandgap of 1T MX ZNRs with ribbon width. Dashed lines represent the band gaps of 2D MXs, and the symbols represent the 1T ZNRs. Colors are consistent to indicate the respective materials.

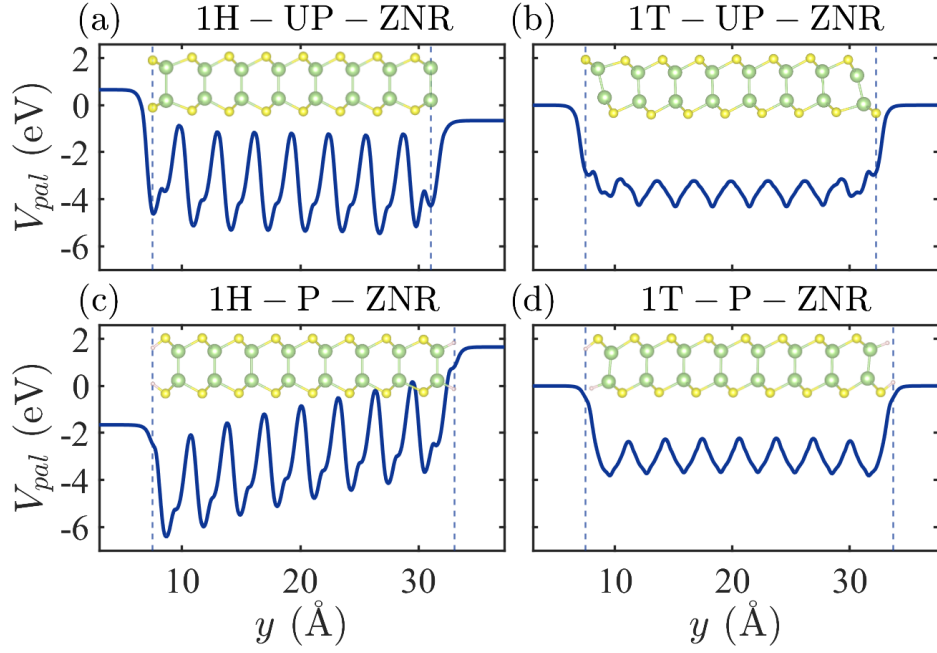


FIG. S4. Planar average of the local electrostatic potential of (a) unpassivated 1H, (b) unpassivated 1T, (c) passivated 1H, and (d) passivated 1T $N = 8$ GaS ZNRs. Vertical dashed lines show the position of the first and last atom along the width of the NRs.

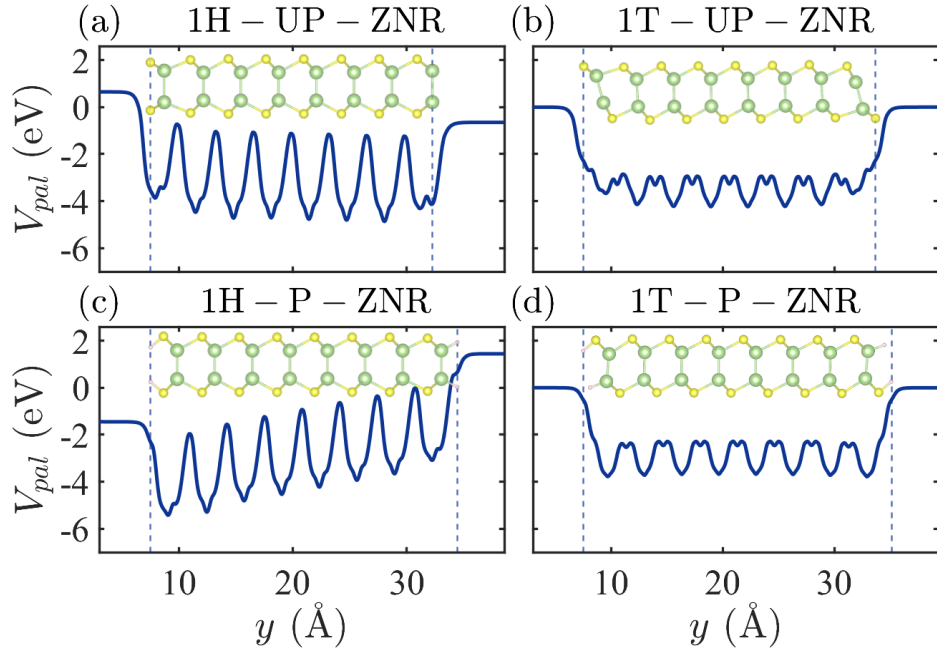


FIG. S5. Planar average of the local electrostatic potential of (a) unpassivated 1H, (b) unpassivated 1T, (c) passivated 1H, and (d) passivated 1T $N = 8$ GaSe ZNRs. Vertical dashed lines show the position of the first and last atom along the width of the NRs.

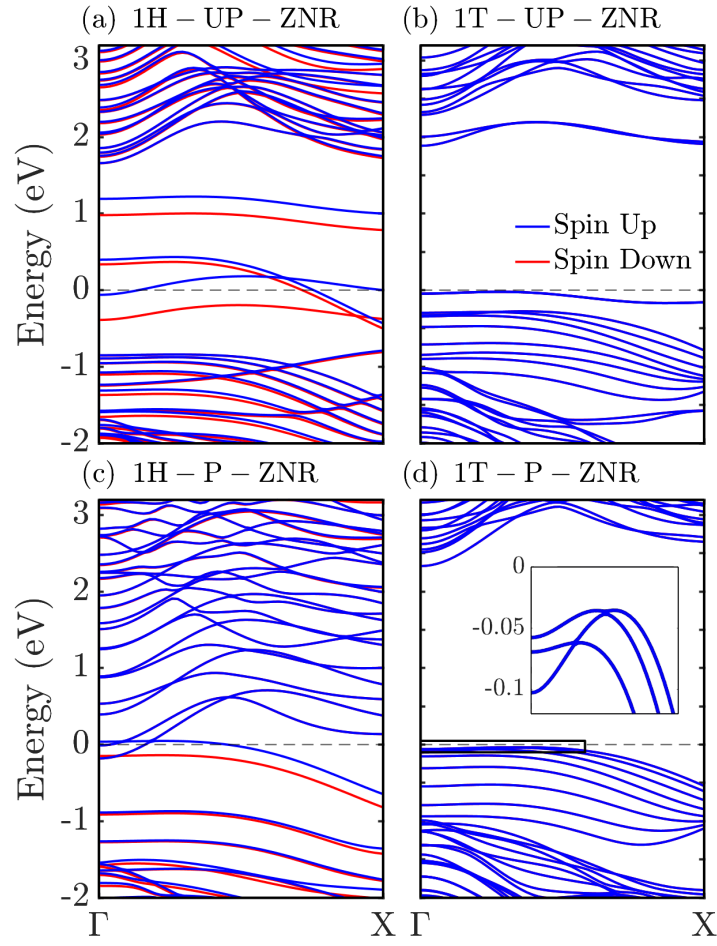


FIG. S6. Spin-polarized band structures of (a) passivated 1H, (b) passivated 1T, (c) unpassivated 1H and (d) unpassivated 1T $N = 8$ GaS ZNRs.

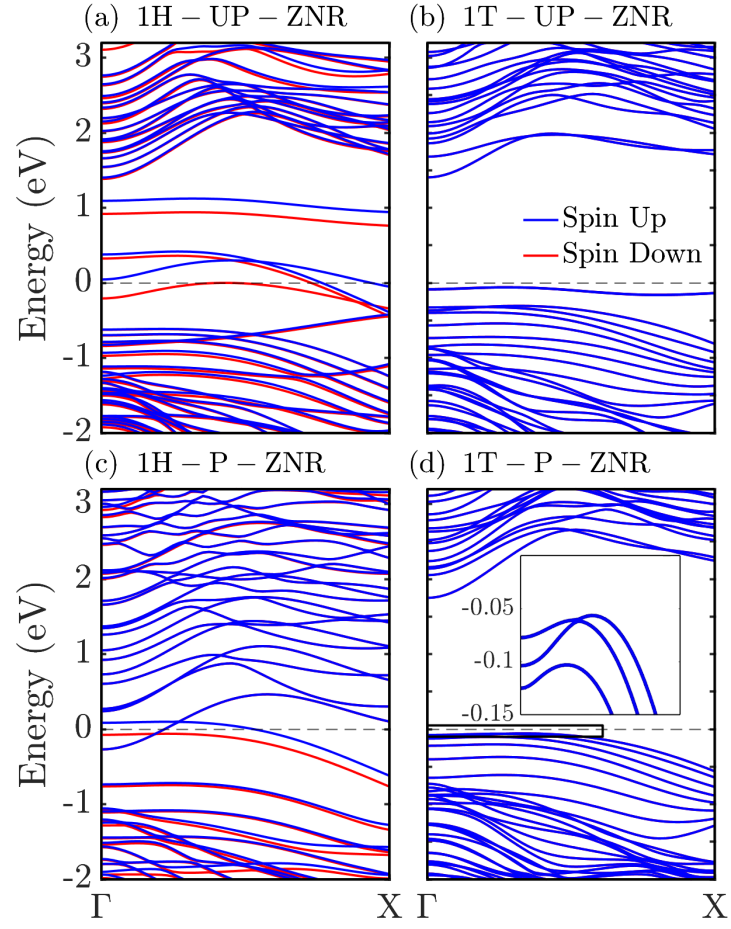


FIG. S7. Spin-polarized band structures of (a) passivated 1H, (b) passivated 1T, (c) unpassivated 1H and (d) unpassivated 1T $N = 8$ GaSe ZNRs.

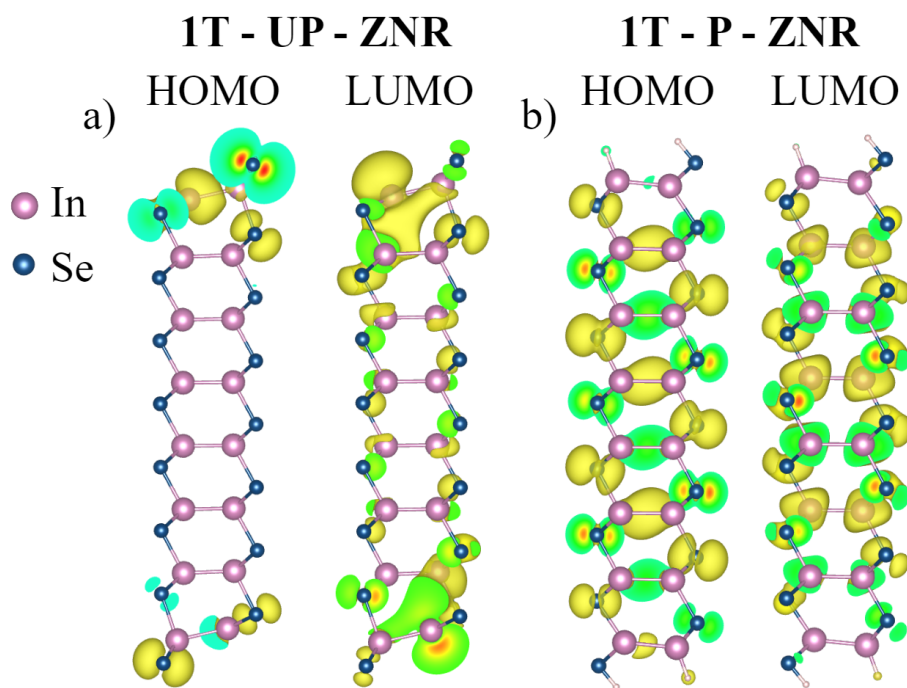


FIG. S8. Partial charge distribution of the HOMO and LUMO bands of (a) unpassivated 1T and (d) passivated 1T $N = 8$ InSe ZNRs.